AD-A163 646 CURRENT DISTRIBUTION IN ESD (ELECTRON STIMULATED DESORPTION) DIODES CROSS SECTION CORRECTIONS(U) CHICAGO UNIV IL JAMES FRANCK INST J C LIN ET AL. NOV 85 4 1/1

UNCLASSIFIED N00014-77-C-0018 F/G 9/1 NL

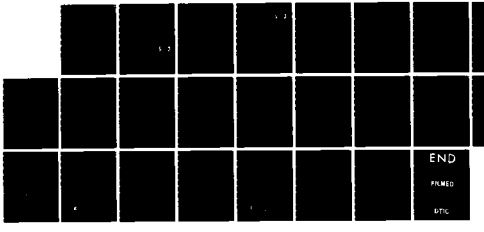

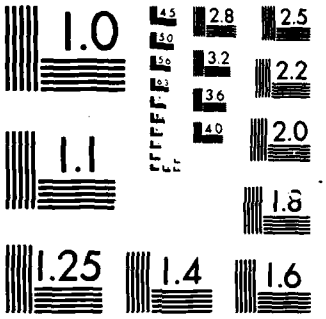

unclassified

SECURITY CLASSIFICATION OF THIS PAGE (When Data Entered)

(12)

AD-A163 646

REPORT DOCUMENTATION PAGE		READ INSTRUCTIONS BEFORE COMPLETING FORM
1. REPORT NUMBER: 4	2. GOVT ACCESSION NO.	3. RECIPIENT'S CATALOG NUMBER
4. TITLE (and Subtitle): Current Distribution in ESD Diodes. Cross Section Corrections		5. TYPE OF REPORT & PERIOD COVERED
		6. PERFORMING ORG. REPORT NUMBER
7. AUTHOR(s): J. C. Lin and R. Gomer		8. CONTRACT OR GRANT NUMBER(s): ONR N00014-77-C-0018
9. PERFORMING ORGANIZATION NAME AND ADDRESS: The University of Chicago, The James Franck Institute, 5640 South Ellis Ave., Chicago, IL 60637		10. PROGRAM ELEMENT, PROJECT, TASK AREA & WORK UNIT NUMBERS
11. CONTROLLING OFFICE NAME AND ADDRESS: Office of Naval Research, Physical Sciences Division, 800 N. Quincy Str., Arlington, VA 22217		12. REPORT DATE: November 1985 13. NUMBER OF PAGES: 31
14. MONITORING AGENCY NAME & ADDRESS (if different from Controlling Office)		15. SECURITY CLASS. (of this report): unclassified 15a. DECLASSIFICATION/DOWNGRADING SCHEDULE

16. DISTRIBUTION STATEMENT (of this Report)

This document has been approved for public release and sale; its distribution is unlimited.

17. DISTRIBUTION STATEMENT (of the abstract entered in Block 20, if different from Report)

18. SUPPLEMENTARY NOTES

Prepared for publication in Surface Science.

19. KEY WORDS (Continue on reverse side if necessary and identify by block number)

Electron Stimulated Desorption, Excitation Cross sections.

20. ABSTRACT (Continue on reverse side if necessary and identify by block number)

The electron current distribution in diodes consisting of a rectangular crystal and an electron emitting filament parallel to and in front of it, used in several electron stimulated desorption (ESD) experiments has been determined by means of a dummy crystal constructed from uniformly transparent Lektromesh and a moveable, suitably constructed fine probe. It was found that for straight filaments the distribution was uniform along the narrow, but nearly triangular along the long dimension of the crystal. Calculated log signal vs. time curves in ESD show con-

DD FORM 1 JAN 73 1473

unclassified

SECURITY CLASSIFICATION OF THIS PAGE (When Data Entered)

siderable curvature, as often observed experimentally with such geometries. Filaments with a straight center, but coiled and shielded end sections provide uniform current distributions. When such filaments are used the curvature of the log signal vs. t curves disappears for Kr desorption from W(110) but is still seen for oxygen desorption. The absolute fraction of filament current hitting the front surface of a crystal was also determined for various geometries by using a thin suppressor mesh in front of the dummy crystal. Cross sections for CO, O, and Kr ESD from W(110) were redetermined with a coiled end section filament. After correction for the fractions of current to the crystal and current nonuniformities previous results are in fairly reasonable agreement with the new values, except for the CO measurements of Leung, Vass, and Gomer, which are still high by a factor of 5. The new measurements permit a recalculation of excitation cross sections for neutral desorption. It is found that the latter are substantially smaller than corresponding gas phase values.

CURRENT DISTRIBUTION IN ESD DIODES. CROSS SECTION CORRECTIONS

J. C. Lin and R. Gomer

Department of Chemistry and
The James Franck Institute
The University of Chicago
Chicago, Illinois 60637

ABSTRACT

The electron current distribution in diodes consisting of a rectangular crystal and an electron emitting filament parallel to and in front of it, used in several electron stimulated desorption (ESD) experiments has been determined by means of a dummy crystal constructed from uniformly transparent Lektromesh and a moveable, suitably constructed fine probe. It was found that for straight filaments the distribution was uniform along the narrow, but nearly triangular along the long dimension of the crystal. Calculated log signal vs. time curves in ESD show considerable curvature, as often observed experimentally with such geometries. Filaments with a straight center, but coiled and shielded end sections provide uniform current distributions. When such filaments are used the curvature of the log signal vs. t curves disappears for Kr desorption from W(110) but is still seen for oxygen desorption. The absolute fraction of filament current hitting the front surface of a crystal was also determined for various geometries by using a thin suppressor mesh in front of the dummy crystal. Cross sections for CO, O, and Kr ESD from W(110) were redetermined with a coiled end section filament. After correction for the fractions of current to the crystal and current nonuniformities previous results are in fairly reasonable agreement with the new values, except for the CO measurements of Leung, Vass, and Gomer, which are still high by a factor of 5. The new measurements permit a recalculation of excitation cross sections for neutral desorption. It is found that the latter are substantially smaller than corresponding gas phase values.

INTRODUCTION

Many investigations of electron stimulated desorption use a hot W or other filament as electron source parallel to and a few millimeters in front of the crystal from which ESD is to be obtained. To our knowledge no measurements of the actual current distribution or the fraction of current hitting the front of the crystal rather than its back or its leads have been made. We report here measurements of the distribution and of the fraction of current hitting the front surface of the crystal. Both questions addressed here have important bearing on the absolute values of cross sections. The current distribution also affects the time evolution of desorption signals and this has considerable bearing on the mechanisms which must be postulated for ESD. Finally, in experiments where conversion to a new species is being investigated it is generally not practical to use a finely focussed beam of electrons, since the entire surface needs to be uniformly illuminated with electrons. For these purposes the diode arrangement is extremely convenient.

EXPERIMENTAL

Current Distributions

One set of measurements was performed in the apparatus shown in Fig. 1. The set-up simulated as closely as possible the geometry used in most of our past ESD experiments [1]. The crystal was simulated by a 3 x 14mmm piece of Mo or Ni Lektromesh foil of $\sim$70% transmission. The electron source consisted of a 0.00762 cm (0.003") diameter W filament, extending slightly beyond the ends of the crystal. Two beam shaping electrodes, used in the actual ESD experiments were also included. A Pt disk of $\sim$3 cm diameter was placed $\sim$3 cm behind the filament assembly to simulate the first of the grids placed between the ESD assembly and the quadrupole mass spectrometer in the actual experiments. The current probe was located behind the crystal (Fig. 1) and is shown schematically in Fig. 2. It consisted of a 0.025 cm diameter

(0.01") tungsten rod 6 cm long covered with a thin layer of Pyrex glass over all but the last 4mm at either end. This coating was achieved by drawing 10mm Pyrex tubing into a fine capillary which was then slipped over the W rod and heated in a very soft, oxygen free flame.

The coated W rod was then inserted into a 5.5 cm long section of s ainless steel hypodermic syringe tubing of 0.0635 cm (0.025") OD and 0.0318 c (0.0125") ID, in such a way that one bare end of the W probe rod was 1mm inside the stainless steel sheath. The back end of the W probe was sp welded to a fine Ni wire, which in turn was insulated by a thin glass tube. A mall section of pyrex capillary was sealed over the back end of the stainless steel capillary and the glass coating of the W rod in order to fix the latter permanently in position relative to the stainless steel sheath. The probe assembly was attached to a 0.25" OD thin walled stainless steel tube which acted as holder and shield. This in turn was attached to one lead of a 2-lead tungsten-Nonex press seal, the other lead being connected via the Ni wire to the actual probe. The front end of the probe was left bare over 4mm in order to prevent charge buildup on the glass insulator from affecting results. No charging effects could be seen. Both the filament assembly and the probe were mounted on stainless steel bellows to allow changing the position of filament and probe. All these components were contained in a conductivized Pyrex bulb of 8 cm diameter attached via a Conflat flange to an Ultek ion pump of 20 ℓ/sec pumping speed. Experiments were carried out only at pressures of $< 10^{-9}$ torr. During most measurements the filament - "crystal" distance was 3-5mm and the probe was just not touching the "crystal". The crystal, the probe, and its sheath were all kept at the same potential. The effective length of the probe (i.e. from the center of the bellows to its end was 14 cm, so that the variation in probe current resulting from the slant of the probe at the extremes of the crystal was entirely negligible.

A second, similar set of measurements was performed in a tube simulating the experimental arrangement used in earlier ESD work by Leung, Vass, and Gomer [2] (LVG), in which the filament and crystal were mounted on the same tungsten glass press seal.

Crystal Current

The fraction of emitted current reaching the crystal rather than the leads and other portions of the apparatus was also determined, using the apparatus shown in Fig. 3. In each case the "crystal" was a piece of Pt foil, 3 x 14mm, whose rear side was protected as shown by a shield, 0.5mm behind it. Reemission of secondaries from the front surface of the "crystal" was prevented by a grid, ca. 1mm in front of the crystal. The latter consisted either of a single piece of 70% transmission Mo Lektromesh foil or of a double grid formed by spotwelding stainless steel mesh on both sides of a 0.5mm (0.020") diameter Pt wire frame, 16 x 4mm. The transmission of the double mesh was determined optically to be 64% ± 1% over its length. Similar measurements using the same shielded "crystal" were also made to simulate the LVG set-up.

RESULTS AND DISCUSSION

Current Distribution

Current distributions along and across the crystal for the apparatus of Fig. 1 are shown in Figs. 4a and 4b. Distributions along the major axis of the crystal were taken at the center line of the crystal while distributions across the crystal were taken at the various x positions indicated. With crystal and envelope at ground (corresponding approximately to the situation used in most actual experiments the distribution across

the crystal was virtually uniform when the steering electrodes were close to filament voltage (V_{fil}-3 volts) for all but low filament to crystal voltages. When the steering electrodes were made negative with respect to the filament, by $\geqslant$ 25 volts, the transverse current distribution showed a minimum near the center line with high values at the edges. A similar transverse distribution was found when the crystal and envelope were kept at ground but the filament-crystal voltage was 30 volts or less.

The longitudinal current distribution in all cases peaked near the center of the crystal and was almost triangular in shape, with a half width (at 10% of maximum intensity) of $\sim$5mm. This resulted from the fact that the filament ends extended only a short distance beyond the crystal so that the temperature of the filament was highest at its center (which almost but not quite coincided with the center (x = 7mm) of the crystal in the dummy arrangement.

To verify this last point experiments were also carried out with a filament consisting of a straight section over the length of the crystal and 2 tightly coiled sections of $\sim$2-3 cm (if uncoiled) length each beyond the crystal. With this arrangement essentially uniform longitudinal distributions were obtained for various y positions.

It is possible to treat analytically the desorption signal vs. time behavior to be expected from a longitudinal triangular current distribution, constant in the transverse direction. We assume a single (total) desorption cross section, σ, and a signal, s, ionic or neutral, whose amplitude is

proportional to the total coverage of desorbing or converting adsorbate remaining on the surface. Then

$$(s/k) = 2wN_o\sigma \int_{-a}^{o} j(x)\, e^{-j(x)\sigma t}\, dx \qquad (1)$$

Here k is the proportionality between actual total desorption (and/or conversion) rate $-\int_A^{o\bullet} \dot{N} dA$ and the observed signal; N_o is the initial coverage in atoms/cm^2; w is the width of the crystal, and j(x) is the current density in electrons/cm^2, assumed to be uniform over the width w of the crystal, but triangular over the long dimension, x, extending from $-a \leq x \leq a$:

$$\begin{aligned} j(x) &= c(x + a) \quad -a \leq x \leq 0 \\ &= c(x - a) \quad 0 \leq x \leq a \end{aligned} \qquad (2)$$

with c easily seen to be

$$c = \frac{i}{wa^2} \qquad (3)$$

where $\underline{i}$ is the total current to the crystal.

It is then straightforward to show that

$$\ln (s/k) = \ln \left(\frac{1 - e^{-\bar{j}\sigma t}(\bar{j}\sigma t + 1)}{t^2} \right) \qquad (4)$$

where

$$\bar{j} = \frac{i}{wa} \qquad (5)$$

and

$$\left. \frac{d \ln s}{dt} \right|_{t = 0} = \frac{4}{3} \sigma \frac{i}{A_i} = \frac{2}{3} \sigma \bar{j} \qquad (6)$$

where

$$A_i = 2wa \qquad (7)$$

is the portion of the crystal area on which electrons impinge. Thus, if the initial slope of the ln s vs. t curve is used to find σ

$$\sigma_{true} = \frac{3}{4} \left(\frac{a}{a_o}\right) \sigma_{app} \qquad (8)$$

where a_o is the half-length of the crystal. In the present case $a/a_o = 0.71$ so that, assuming the total emission current to hit the front surface of the crystal, apparent initial cross sections σ_{app} must be multiplied by 0.53 to correct for the effect of non-uniform current distribution. Eqs. (6) can also be derived directly from Eqs. (2) and (3) and

$$\left.\frac{d \ln s}{dt}\right|_{t = 0} = \frac{\sigma \int_{-a}^{o} j^2(x)\, dx}{\int_{-a}^{o} j(x)\, dx} \tag{9}$$

which follows from Eq. (1).

It is also interesting to plot log s vs. t, as shown in Fig. 5 for various assumed values of $\bar{j}\sigma$. These plots display some curvature which increases with $\sigma\bar{j}$, simulating two desorption regimes with differing σ values. In a previous publication such behavior for the electron stimulated desorption of Kr from a W(110) surface was interpreted in terms of rather complex desorption kinetics [1]. Figure 6 shows an experimental plot of log s vs. t for Kr/W(110) ESD obtained with a straight filament, i.e. a non-uniform current distribution, and the best fit to Eq. 4. We will show in a subsequent section that single, straight lines result from Kr desorption when uniform current distributions are used.

Non-uniformity may also be of some importance when an electron gun rather than a filament is used, if the beam does not have a rectangular profile. For a current density given by

$$j(r) = c\, e^{-(r/b)^2} \tag{10}$$

it is straightforward to show that

$$\left.d\ln s/dt\right|_{t = 0} = \frac{\sigma i}{\sqrt{2}\, \pi\, b^2} \tag{11}$$

where i is the total current to the crystal. The ln s vs. t behavior, however, must be obtained numerically.

For a conical distribution, i.e. a triangular current profile axially symmetric about the crystal normal it can be shown that

$$\left.\frac{d \ln s}{dt}\right|_{t = 0} = \frac{3\sigma i}{2\pi a^2} \tag{13}$$

where a is half the base width of the triangular distribution.

In the LVG arrangement triangular distributions along the length of the crystal were found as before, but the distribution across the crystal was also triangular, (Figs. 7a and 7b). Thus tne current hit a much smaller area and apparent cross sections were therefore higher. For triangular distributions along the x and y directions the true and apparent initial cross sections are found to be

$$\sigma_{true} = \sigma_{app} \frac{9}{4} \frac{ab}{A_{tot}} \tag{13}$$

where a and b are half the base widths of the distributions along the x and y directions, respectively. The measured values of a and b are 3.5 and 1mm so that the initial cross sections reported by these authors must be multiplied by a factor of 0.19.

Crystal Current

a. Straight Filaments

For the set-up of Fig. 3 simulating the arrangement of Ref. 1, with a straight filament and suppression of secondaries by the mesh, the current reaching the front surface of the crystal was found to be 44% for a crystal-filament voltage of 150 volts, with the crystal near ground and 49% with the filament near ground (i.e. envelope potential). For a crystal-filament voltage of 30 volts the fraction increased considerably and was sensitive to the specific arrangement used: With the crystal at ground 53% of total current hit the front surface of the crystal for crystal-filament distances of 5mm. With the filament grounded the current to the front face of the crystal was 83% of the total for a crystal-filament separation of 5mm.

Measurements simulating the LVG arrangement indicated that 100% of emitted current reached the front surface of the crystal. This is plausible because (a)

the electrical arrangement precludes electrons hitting the envelope, and and (b) the filament support wires just outside the crystal leads confine electrons to the crystal; this conclusion is also borne out by the current distribution measurements presented in the last section.

Experiments with an unshielded crystal and one lead disconnected also gave some interesting conclusions. With the crystal at ground (envelope) and the filament at -150 volts the apparent crystal current (corrected by subtracting the current to the disconnected lead) is 23%. Assuming a secondary electron correction of 100% this yields an incident current of 46%, in good agreement with the shielded crystal results. When the crystal is kept at 150 volts with the filament at ground, so that no secondaries can reach the envelope the current to the crystal and its single lead is 66%, that to the open lead 33%, which makes the apparent crystal current 33%. In this case secondaries are still emitted from the crystal but a larger fraction apparently reach the leads than when the crystal is at ground, or negative with respect to the envelope. For the LVG arrangement, however, 100% of total current reaches the crystal, in agreement with the previous conclusion.

Total initial decay cross sections for Kr and CO were measured in the actual apparatus with the crystal either at ground or 150 volts, using a straight filament and steering electrodes. For instance for Kr with the crystal at ground or -22.5 volts for a total filament current of 80 microamperes the apparent crystal plus lead current was 39.5 microamperes, which compares well with 44% of the total current, 35.2 microamperes. If this latter value is used to calculate a cross section from the decay of the Kr signal a value of 1.23×10^{-17} cm^2 (uncorrected for current distribution on the crystal) is obtained. With the filament at ground and the crystal at +150 volts, a total current of 80 μ amperes was used. If 49% of this attributed to the

crystal, a cross section of 1.12×10^{-17} cm^2 is obtained. Similar results were found for CO: the apparent cross sections uncorrected for nonuniformity of crystal current are 6.3×10^{-18} cm^2 for the crystal at +22.5 eV, and 7.7×10^{-18} cm^2 for the crystal at 150 volts.

b. Spiral Filaments

Measurements were also carried out for a filament with spiral end sections, both when the latter were left unshielded and when they were shielded by small Pt tabs at filament potential in front of the spiral sections. In the former case steering electrodes were used and the results were essentially identical to those for the straight filament. It was found, however, that the position of the filament with respect to the steering electrodes was quite critical to the uniformity of current distributions and that more uniform distributions could be obtained by replacing the steering electrodes by a circular grid of 2.5 cm diameter a few millimeters behind the filament (i.e. on the opposite side of the filament from the crystal, in the direction of the mass analyzer), kept 0-3 volts negative with respect to the filament. For this arrangement, and with shields for the spiral end sections a much smaller fraction of total filament current hit the front face of the crystal. For the filament kept near ground (envelope potential) the fraction hitting the crystal, is 25% for an electron energy of $\geq$ 60 eV, and then rises rapidly with decreasing energy. When the crystal was kept near ground roughly 10-13% of filament current reached the front face of the crystal for electron energies $\geq$ 60 eV and then increased, the increases depending sensitively on the actual crystal voltage with respect to the envelope.

Experiments in the real apparatus using this arrangement, however, indicated that the slopes of ln s vs. time curves and initial signals were nearly the same when either the crystal or filament were near apparatus ground. The

reason for this is that in the simulated setup the envelope was physically much closer to the crystal and filament than in the actual apparatus, so that the envelope potential was much more important in the test setup when steering electrodes were not used. The latter largely shield the crystal from the envelope, as indicated by the fact that the envelope potential has very little effect on the fraction of current reaching the crystal when steering electrodes were used. Experiments with the crystal-filament arrangement just described were therefore carried out in the actual apparatus by mounting the dummy crystal and filament assembly on a 6" diameter Conflat flange, inserted into the actual apparatus. With this arrangement the fraction of emitted current hitting the crystal when the crystal-filament voltage was 150 volts was 27.7% with the crystal at +22 volts and 36.4% with the filament near ground in fair agreement with actual cross section measurements made with this arrangement.

Cross Section and Related Measurements

In view of the preceding it was interesting to repeat measurements on Kr, CO, and O adsorbed on W(110) with an electron source providing uniform current distributions. This was done by installing a filament with shielded spiral end sections and a grid behind the filament, as described in the last section.

Results for Kr ESD are shown in Fig. 8. It is evident that there is no curvature in the log (Kr signal) vs. t curves, but that the slopes, i.e. cross sections increase when initial coverage $\theta_i \leq 0.25$. We may therefore conclude that the complex mechanism advanced previously to account for the curvature, namely conversion to a new state, is not valid, but that a single state exists from which desorption occurs without conversion to an electron induced state. The variation of σ with initial θ, however, has no simple explanation. If the effect were solely due to Kr-Kr interactions σ should increase as ESD proceeds and coverage decreases. It is possible that ESD takes place principally from island edges so that these shrink as ESD proceeds, leaving σ constant.

Since there is very little coverage dependence for $\theta_i > 0.25$ it may be that islands exist initially above, but not below this coverage. The σ values are summarized in Table I.

Experiments were also carried out for CO adsorbed on W(110) at 90 K to saturation. The σ values obtained from both the decay of the CO^+ and neutral CO signals are also shown in Table I. In addition it was found that v-CO can be completely converted to β-CO, in that there is no virgin-CO peak in thermal desorption after ESD to the disappearance of the CO^+ signal. Additionally, the work function increment, measured with a vibrating Kelvin diode to be described in more detail elsewhere [3] changed from $\Delta\phi \cong 1.0$ eV for saturated v-CO to $\Delta\phi = 0.425$ eV after ESD, which is reasonably close to the value $\Delta\phi = 0.370$ eV, obtained for β-CO by heating a virgin layer to 400 K. The present results also explain why Opila and Gomer [4] saw some v-CO in UPS and XPS after disappearance of the CO^+ signal, rather than a new electron induced state. Electron impact, as the present results indicate, leads either to desorption or conversion to β-CO. If the current distribution is non-uniform, however, the CO^+ signal will be quite small when there is still v-CO left on the portions of the crystal receiving only a low electron flux, but such v-CO will show up in XPS which illuminates essentially the whole crystal surface, and also in UPS, which illuminates only a rather small spot, if the latter happens to not coincide with the maximum of the current distribution. This can easily happen if either the photon beam or the maximum of the electron density do not coincide with the center of the crystal.

Oxygen adsorbed to saturation at 90 K, corresponding to $O/W \cong 0.6$ was also subjected to ESD with the new arrangement. The results, shown in Fig. 9 indicate that there are still 2 regimes with 2 distinct cross sections, which are also listed in Table I. In the case of O/W(110) only an O^+ but no neutral O signal could be seen. This suggests either that there is only

conversion not desorption of neutral O, or that desorbing O has sufficient kinetic energy to pass through the ionizer of the mass analyzer so rapidly that it cannot be ionized with sufficient efficiency for detection.

Corrections to Previous Measurements

We are now in a position to make at least first order corrections to measurements carried out with a straight filament and then to compare them with those carried out with uniform current distributions. Since the corrections arising from non-uniformity of current distributions hold strictly speaking only at t = 0, i.e. correct the initial slope these corrections will probably not be totally accurate. The uncorrected and corrected values for σ_{CO} and σ_{O} obtained by LVG [2] and by Leung, Steinbrüchel and Gomer [5], Opila and Gomer [4], and the present authors with nonuniform current distributions as well as the values obtained by the new setup, discussed in the last section are all listed in Table I, which includes also the Kr cross sections of Ref. 1 as well as those obtained in the present work.

It appears from Table I that the corrected results of LVG [2] for CO are higher by a factor of 5 than the present results, using uniform current distributions. For O the corrected values from Ref. 5 are apparently high by only a factor of $\sim$2. It is possible that some of the error in the CO results arises from residual carbon or from even more compression of the electron beam in the actual LVG apparatus than in the test setup. In general the corrected nonuniform current distributions give slightly higher cross section values than uniform distributions. This may be due in part to the fact that the absolute fraction of crystal current for the arrangement used by Opila and Gomer [4] and by Zhang, Gomer, and Bowman [1], i.e. using steering electrodes, was measured only in the 8 cm diameter test bulb. The value obtained may be too small, thus giving too high corrected cross sections. In any case the discrepancies

are not very large: for CO and O it is a factor of ∿2, while for Kr it is 1.7.

It is also interesting that in the present experiments slightly higher values are consistently seen when the total disappearance cross section of CO is measured by following the neutral CO rather than the CO^+ signal. This suggests that as desorption and conversion to β-CO occurs by electron impact, the ratio of CO/CO^+ decreases slightly, possibly because CO^+ neutralization decreases or because of a slight change in excitation cross sections for the two processes.

Corrections to Excitation Cross Sections

It was shown previously [5] that isotope experiments allow one to dissect total desorption cross sections σ into excitation cross sections σ_e and desorption probabilities P. If σ is written

$$\sigma = \sigma_e P \tag{14}$$

and

$$P = e^{-cM^{\frac{1}{2}}} \tag{15}$$

$$c = \frac{\ln(\sigma_1/\sigma_2)}{M_2^{\frac{1}{2}} - M_1^{\frac{1}{2}}} \tag{16}$$

where M is mass in a.m.u. and the subscripts stand for different isotopes. Since the constant c depends only on ratios of cross sections, values of P determined previously should be valid as long as the errors in σ are the same for different isotopes. We are thus able to obtain new σ_e values on the basis of the present results from previous values simply by using the correction to the total cross sections. σ_e values so found are listed in Table II.

Cross sections for ion formation are based on ion/electron yield ratios. Excitation cross sections are obtained by combining these data with ion yield ratios for different isotopes. The latter were obtained in the apparatus of LVG and probably need no corrections. The former were obtained both in the

apparatus of LVG and also with a retarding grid system in Ref. 5, using a Leed gun as electron source. The i_+/i_- values obtained with the grid system are probably more reliable and we have listed in Table II the excitation cross sections for ion production obtained on this basis. These values are taken from Ref. 5, and are shown here for the sake of completeness. It should be noted in this connection that the excitation cross section for Kr desorption is that of ionization although reneutralization makes Kr^o the only observable desorption product.

The data of Table II indicate that for chemisorbed species the excitation cross sections are generally smaller than cross sections for excitations or ionization of gas phase molecules. In view of the complexity of chemisorption bonding this is not surprising. It is also interesting that ionization cross sections can be very small and decrease with bond strength suggesting the possibility that Auger processes may play an important role, as suggested by Knotek and Feibelman [6] or simply that it is hard to make an ion from a covalently bonded ad-complex by any process. It is significant, however, that this is not the case for a physisorbed species like Kr, as also noted previously [1].

ACKNOWLEDGMENT

This work was supported in part by ONR Contract N00014-77-C-0018. We have also benefitted from the Materials Research Laboratory of the National Science Foundation at the University of Chicago.

REFERENCES

[1] Q. -J. Zhang, R. Gomer, and D. R. Bowman, Surf. Sci. 129, (1983), 535.

[2] C. Leung, M. Vass, and R. Gomer, Surf. Sci. 66, (1977), 67.

[3] M. Chelvayohan and R. Gomer, Surf. Sci., submitted.

[4] R. Opila and R. Gomer, Surf. Sci. 129, (1983), 563.

[5] C. Leung, Ch. Steinbrüchel, and R. Gomer, Appl. Phys. 14, (1979), 79.

[6] M. L. Knotek and P. Feibelman, Phys. Rev. B15, (1978), 6578.

Table I

Summary of Some ESD Cross Sections from W(110)

Source	σ(v-CO) (cm^2)	σ(0) cm^2	σ(Kr) (cm^2)
LVG (2), uncorrected	$5x10^{-17}$	$1\text{-}2x10^{-17}$ $^{\neq,**}$	---
LVG (2), corrected[1]	$9.5x10^{-18}$	$2\text{-}3.8x10^{-18}$ $^{\neq,**}$	---
Opila and Gomer (4) corrected[2]	$3.9x10^{-18}$	$2.2x10^{-18*}$	---
Present work, straight filament[3]	$3.8x10^{-18}$	---	$6.3x10^{-18}$ θ_i=1
Present work, spiral end sections[4]	from CO^+ $1.6x10^{-18}$ from CO $1.8x10^{-18}$	$9x10^{-19*}$ $1.5x10^{-18**}$	$3\text{-}3.9x10^{-18}$ θ_i=1
Zhang, Gomer, and Bowman (1) uncorrected	---	---	$4.9x10^{-18}$ θ_i=1
Zhang, Gomer, and Bowman (1) corrected[3]	---	---	$6x10^{-18}$

1) Correction factor 0.19 as explained in text.

2) Corrected for total impinged current and nonuniformity. Correction factor = 1.09.

3) Corrected by assuming $i_{xtal} = 0.44\ i_{fil}$ and using nonuniformity correction.

4) Average of crystal at +22v and at 150v with respect to ground, using the appropriate crystal currents, as explained in text, for CO and Kr. For σ(0) O^+ was only measured with filament at ground.

$^{\neq}$obtained in the LVG apparatus, but published in Ref. (5).

*from slope of initial regime.

**from substracting final from initial regime, as discussed in Ref. (5).

Table II

Corrected Excitation Cross Sections

	Total Disappearance		Ion Formation	
	α_e cm^2	P	σ_e cm^2	P
v-CO*	2.6×10^{-17}	6.6×10^{-2}	4.4×10^{16}	1.5×10^{-6}
α-CO*	2.6×10^{-17}	6.6×10^{-2}	2.3×10^{-17}	10^{-4}
O from β-precusor*	1×10^{-18}	0.2	4.6×10^{-18}	3.8×10^{-3}
O*	4.5×10^{-18}	0.18	1.3×10^{-19}	3.9×10^{-4}
Kr≠	----------		1.6×10^{-16}	0.024

*original data from Ref. 5. Oxygen values from initial minus final regime.

≠original data from Ref. 1.

FIGURE CAPTIONS

1) Schematic drawing of apparatus for determining current distributions. For simplicity of viewing steering electrodes or first grid behind filament have been omitted. These arrangements are shown schematically in inserts (a) and (b) respectively. The conductive coating on the inside of the bulb is also omitted for clarity, as are the bellows adjustment yokes and screws.

2) Details of the current distribution probe. For clarity the spacing between the inside of the stainless steel capillary and the 0.010" W collector rod has been exaggerated.

3) Schematic diagram of the collector assembly used for determining absolute current to the front face of the crystal. A single suppressor mesh only is shown and the glass insulation of the "crystal" support lead has been omitted.

4) Current distributions for a straight filament with steering electrodes. Steering electrodes are -3 volts relative to filament. Crystal at envelope ground, filament at -150 volts. (a) distribution along x direction at center of "crystal". (b) distributions along y direction at various values of x.

5) Plots of log s vs. t based on Eq. (4) for various values of $\bar{j}\sigma$. These are shown next to each curve in units of electrons/second.

6) (x) Semilogarithmic plot of an experimental Kr vs. time signal with a straight filament and steering electrodes. The total actual current impinging on the crystal is 34.4 microamperes. After correction for non-uniformity the calculated cross section is $\sigma = 6.7 \times 10^{-18}$ cm^2. (0) Theoretical curve based on Eq. (4) chosen to provide best match with the experimental curve. $\sigma\bar{j} = 1.15 \times 10^{-2}$ e/sec where σ is cross section and $\bar{j} = i/wa$.

7) Current distributions in the LVG arrangement. All voltages as used by LVG [2]. (a) distributions along the long dimension of the crystal, (b) along the short dimension.

8) Kr ESD results for a filament with spiral end sections and uniform current distribution. Various initial coverages are indicated on the figure. Current density 158 microamperes/cm^2. Cross sections obtained from these curves are as follows: $\theta_i = 1$, $\sigma = 3 \times 10^{-18}$ cm^2; $\theta_i = 0.75$, $\sigma = 3.5 \times 10^{-18}$ cm^2; $\theta_i = 0.5, \sigma = 3.5 \times 10^{-18}$ cm^2; $\theta_i = 0.25, \sigma = 4.8 \times 10^{-18}$ cm^2.

9) Oxygen ESD from W(110) for uniform current density (o) experimental points. (Δ) initial regime based on substracting the long-time regime from the experimental points at short times. Current density 492 microamperes/cm^2. Cross sections are as follows: Initial regime, uncorrected by subtraction of final regime $\sigma = 8.6 \times 10^{-19}$ cm^2; initial regime corrected by substraction of final regime, $\sigma = 1.4 \times 10^{-18}$ cm^2; final regime $\sigma = 2.8 \times 10^{-19}$ cm^2.

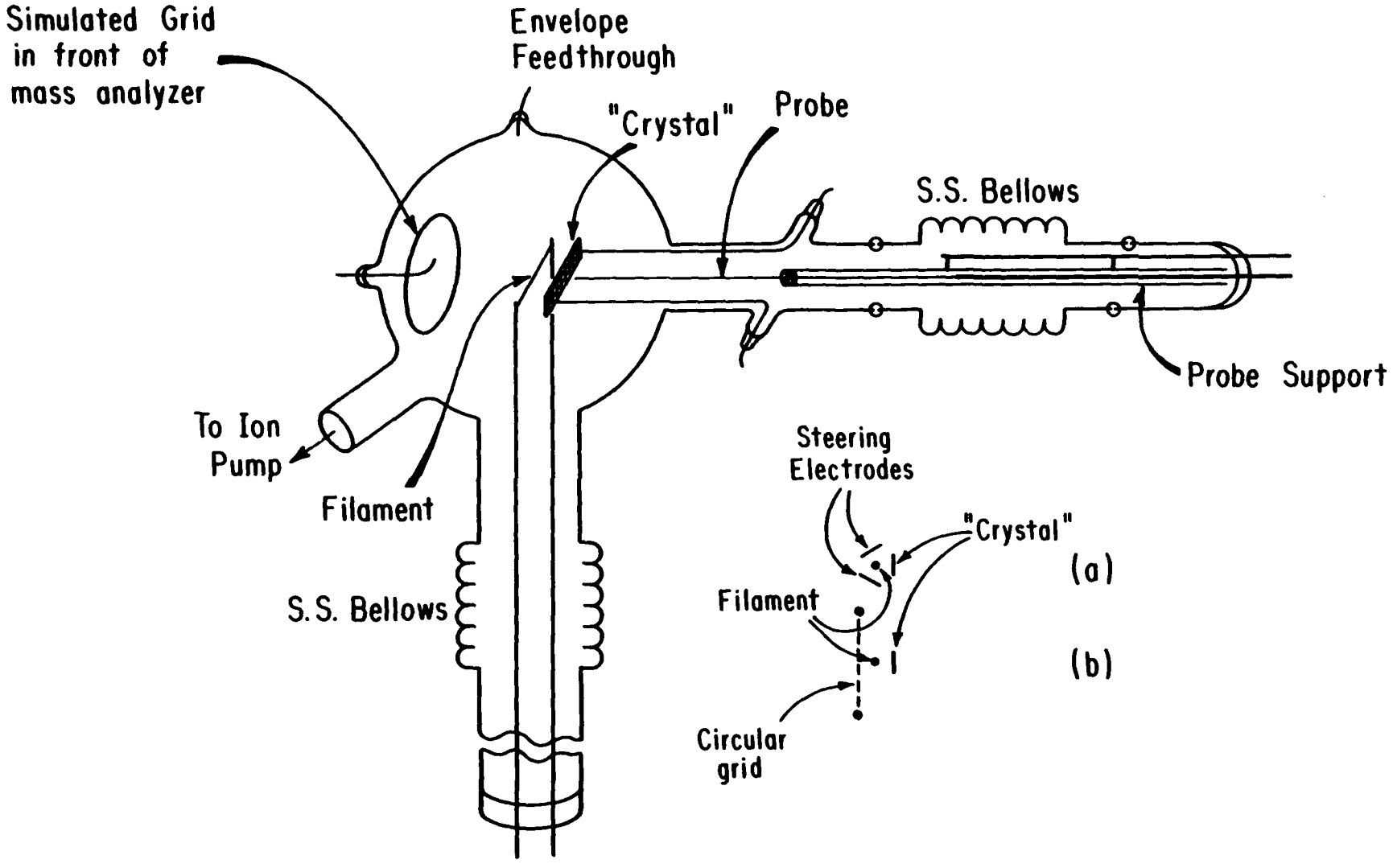
Simulated Grid
in front of
mass analyzer
Envelope
Feedthrough
"Crystal"
Probe
S.S. Bellows
Probe Support
To Ion
Pump
Filament
S.S. Bellows
Steering
Electrodes
"Crystal"
(a)
Filament
(b)
Circular
grid

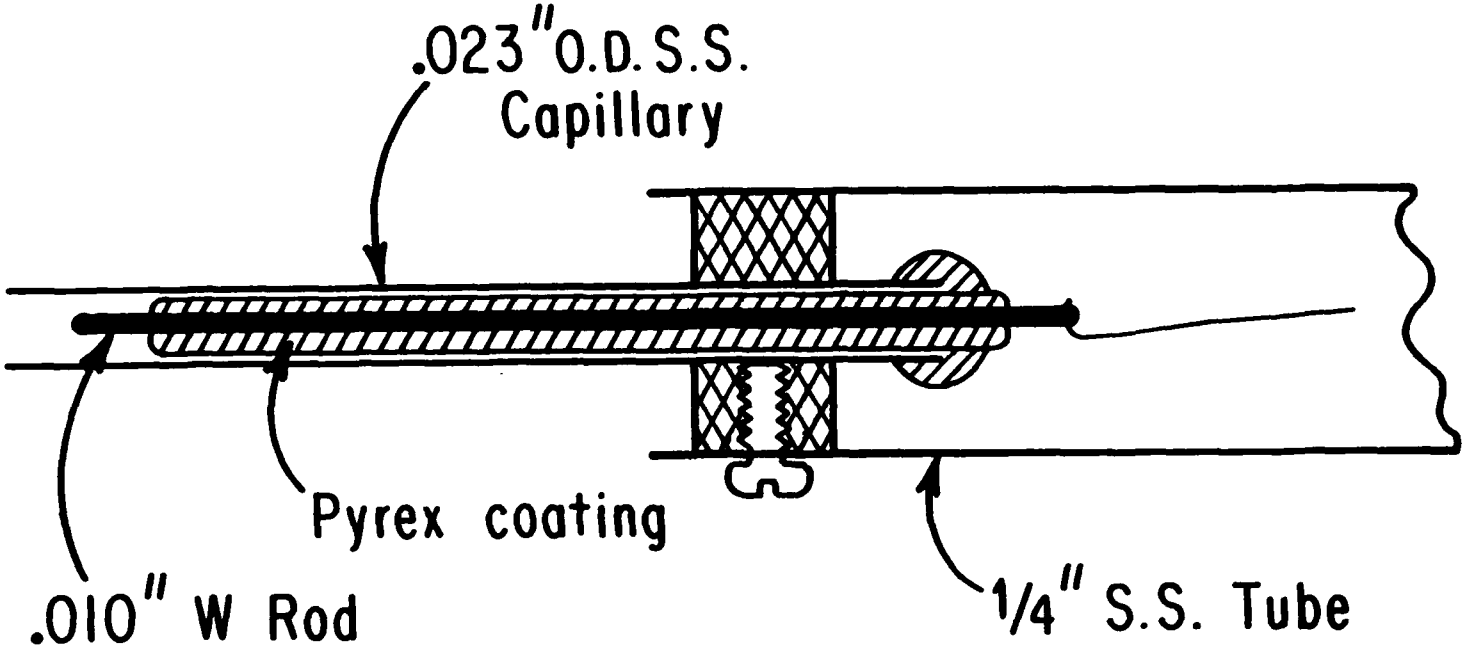

Fig 2.

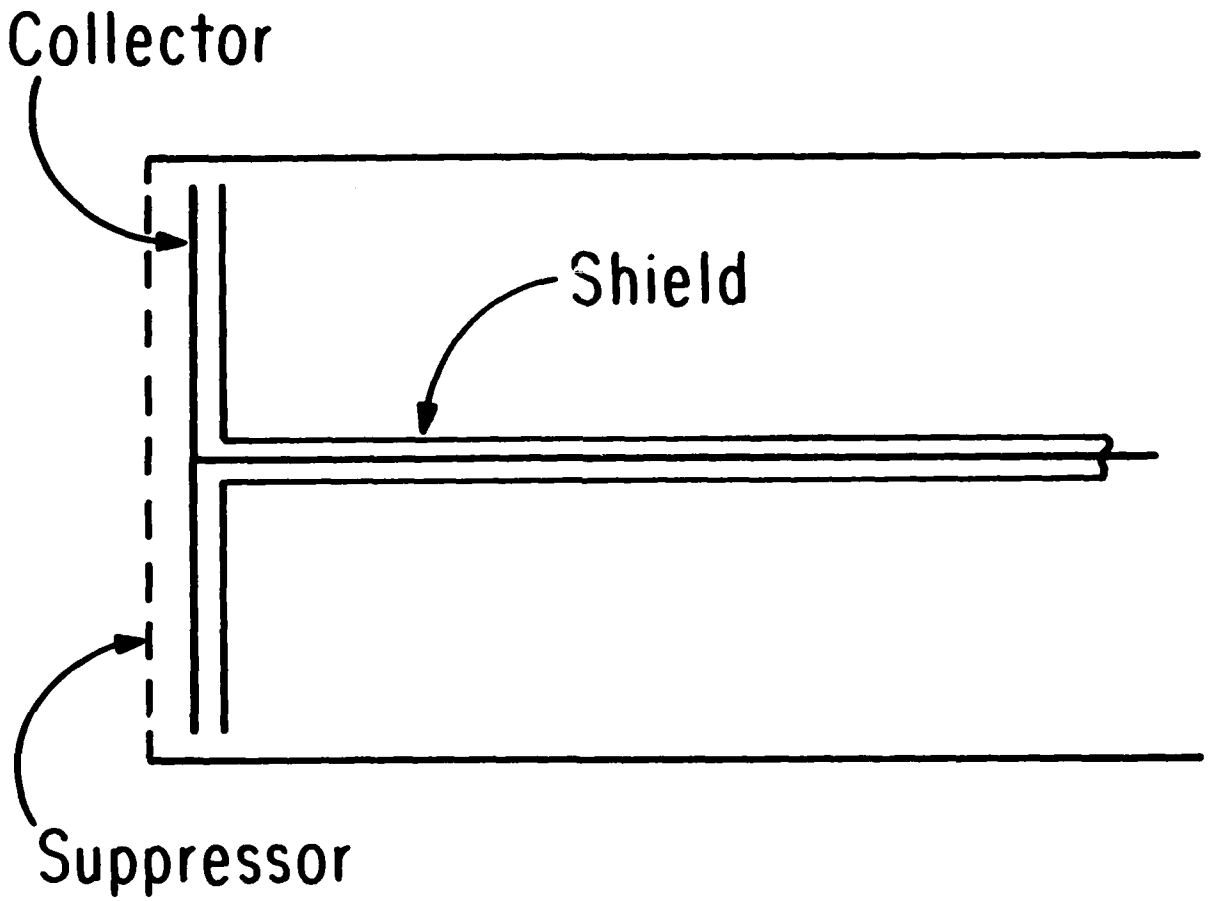

Fig 3

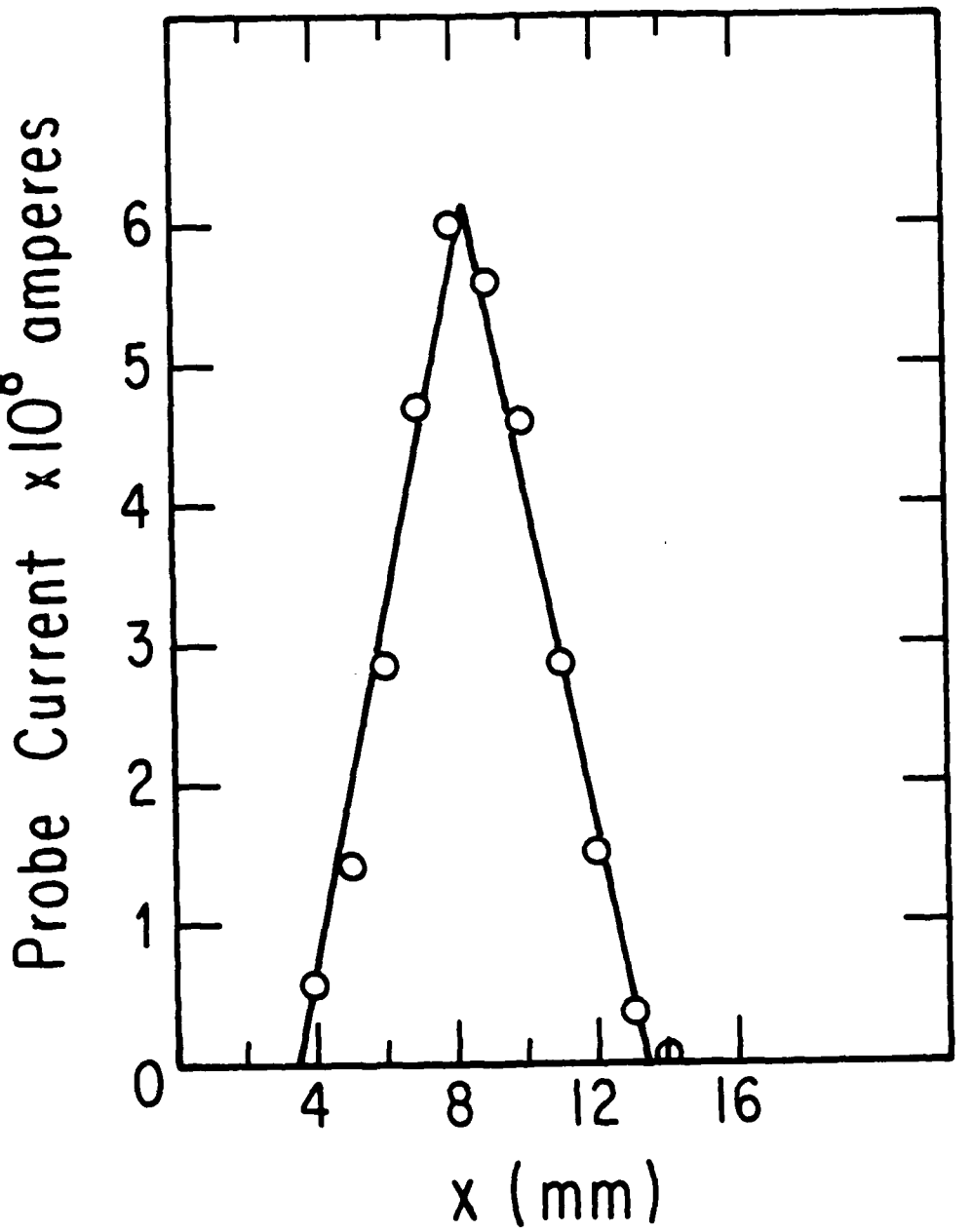

Fig 4a

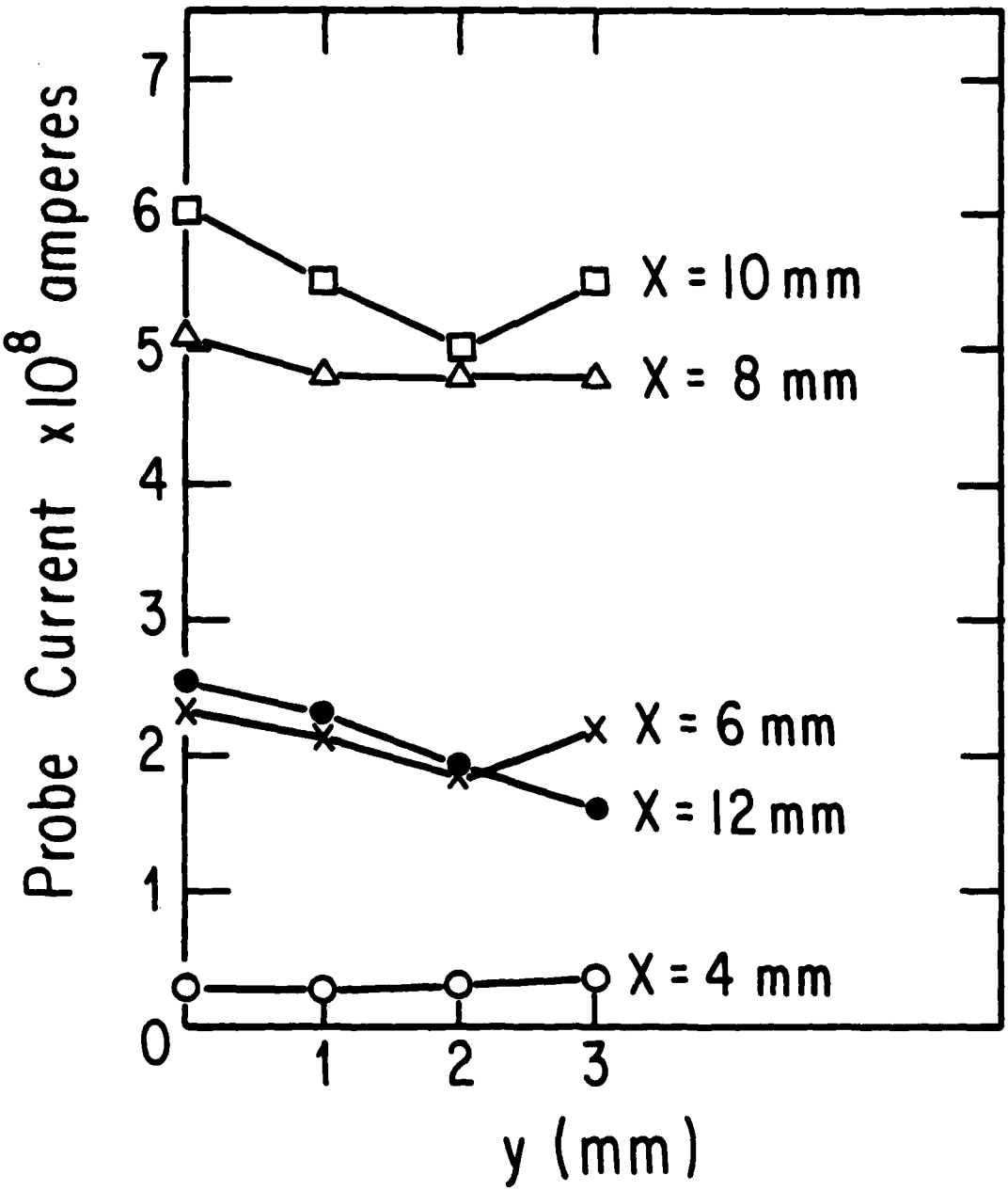
Probe Current x10^8 amperes
7
6
5
4
3
2
1
0
1
2
3
y (mm)
X = 10 mm
X = 8 mm
X = 6 mm
X = 12 mm
X = 4 mm

Fig 4b

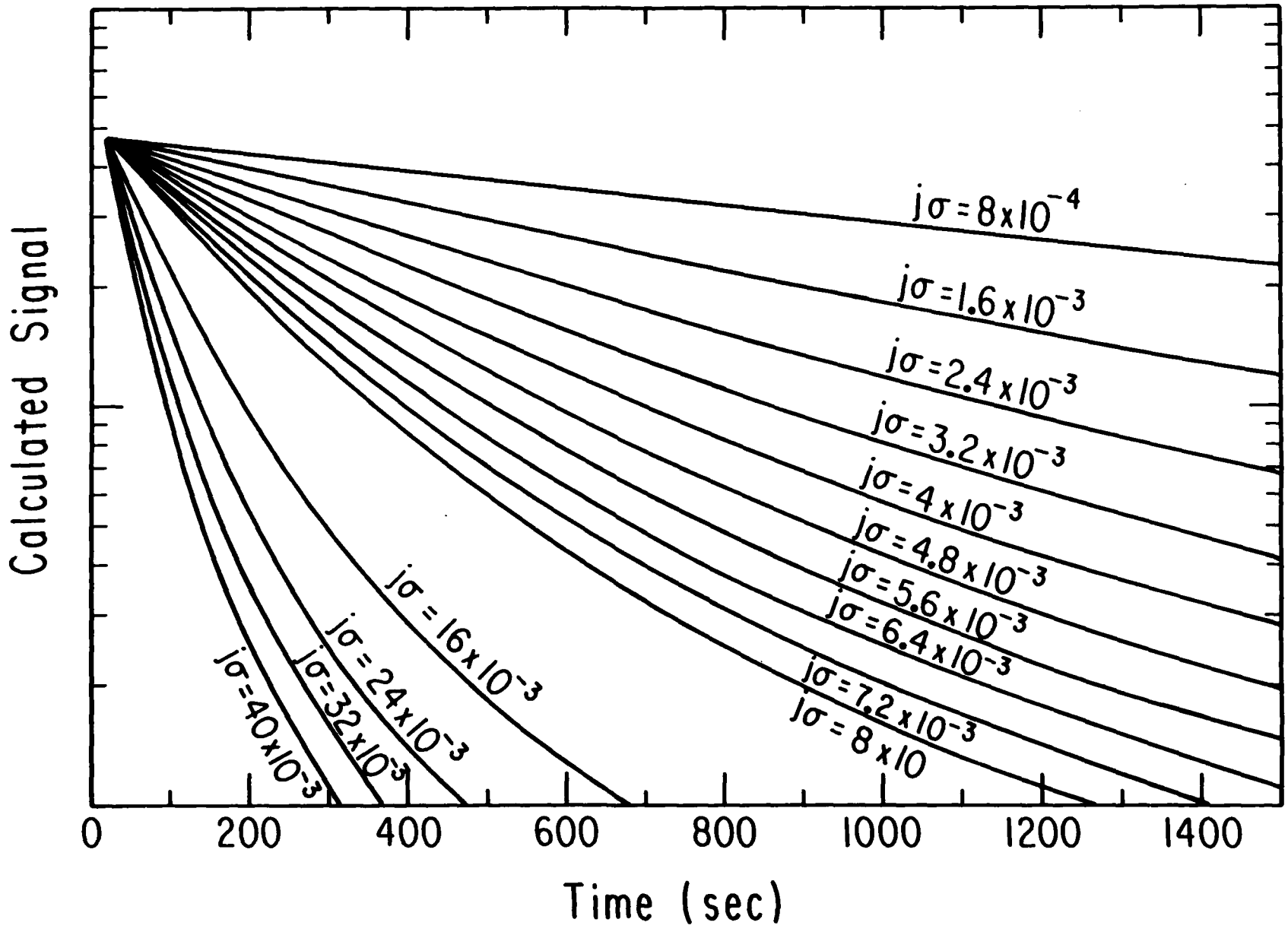
Calculated Signal
Time (sec)
0
200
400
600
800
1000
1200
1400
jσ = 8x10⁻⁴
jσ = 1.6x10⁻³
jσ = 2.4x10⁻³
jσ = 3.2x10⁻³
jσ = 4x10⁻³
jσ = 4.8x10⁻³
jσ = 5.6x10⁻³
jσ = 6.4x10⁻³
jσ = 7.2x10⁻³
jσ = 8x10
jσ = 16x10⁻³
jσ = 24x10⁻³
jσ = 32x10⁻³
jσ = 40x10⁻³

Fig 5.

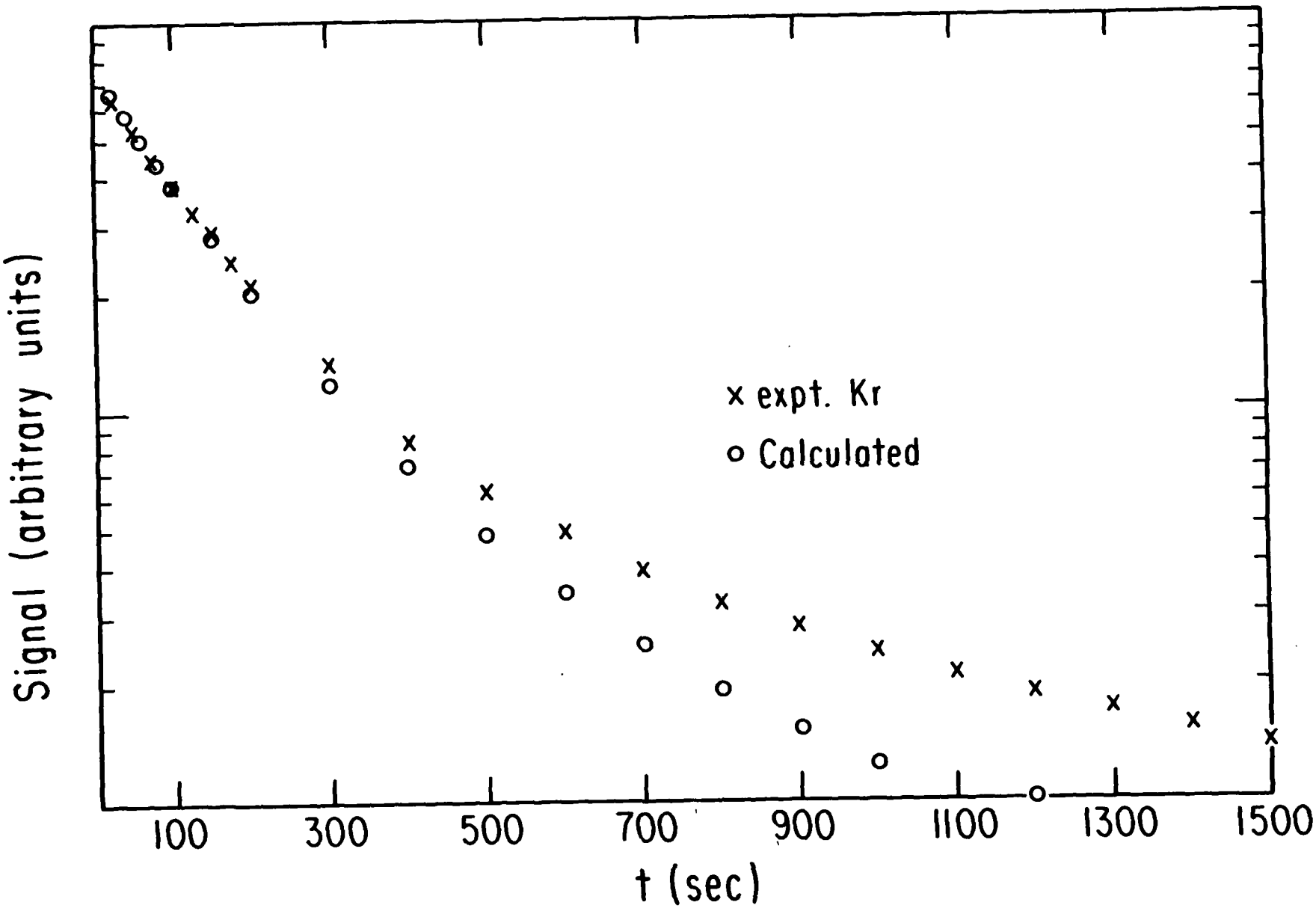
Signal (arbitrary units)
x expt. Kr
o Calculated
100
300
500
700
900
1100
1300
1500
t (sec)

Fig 6

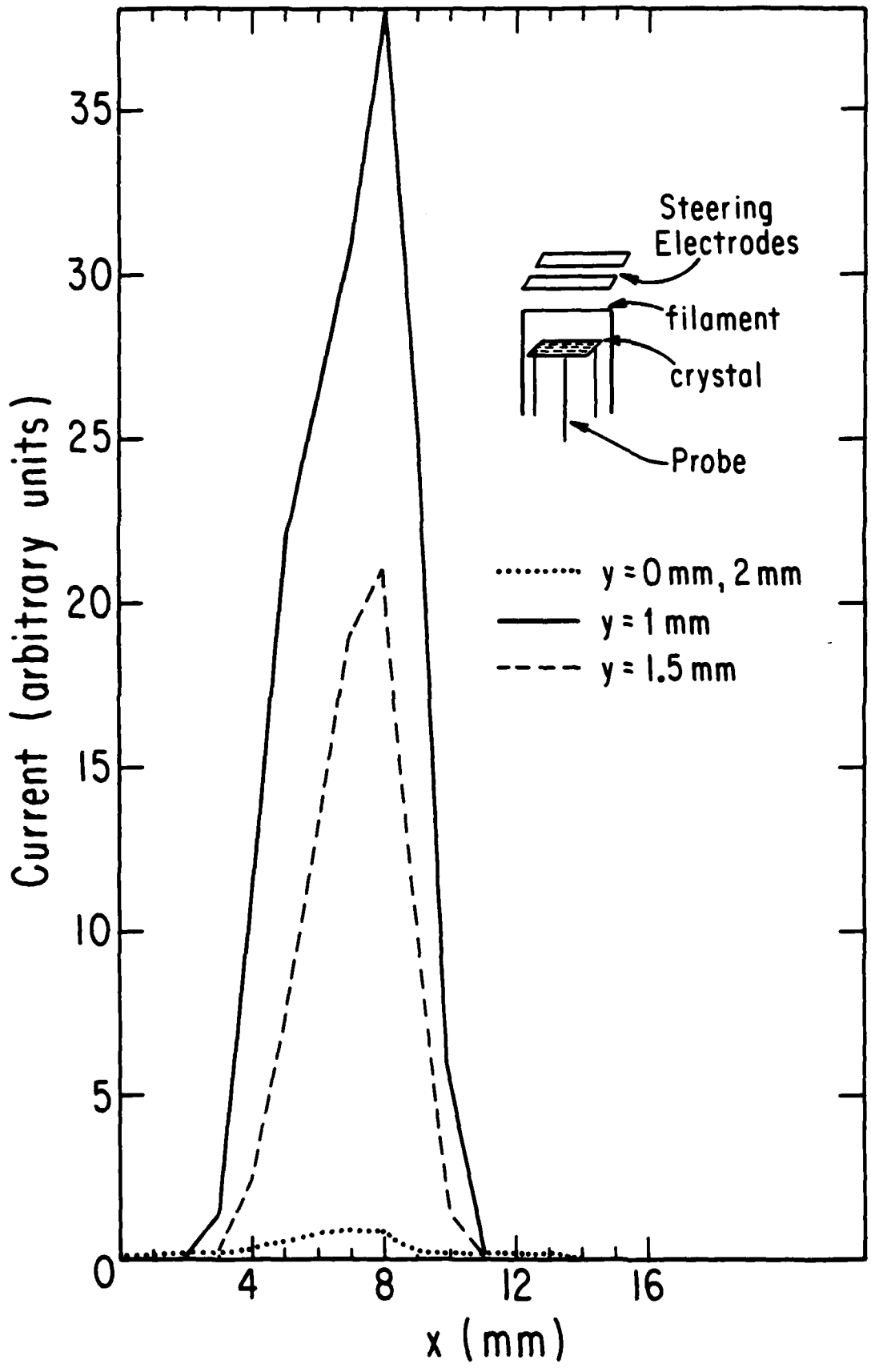
Steering
Electrodes
filament
crystal
Probe
y = 0 mm, 2 mm
y = 1 mm
y = 1.5 mm
Current (arbitrary units)
0
5
10
15
20
25
30
35
4
8
12
16
x (mm)

Fig 7a

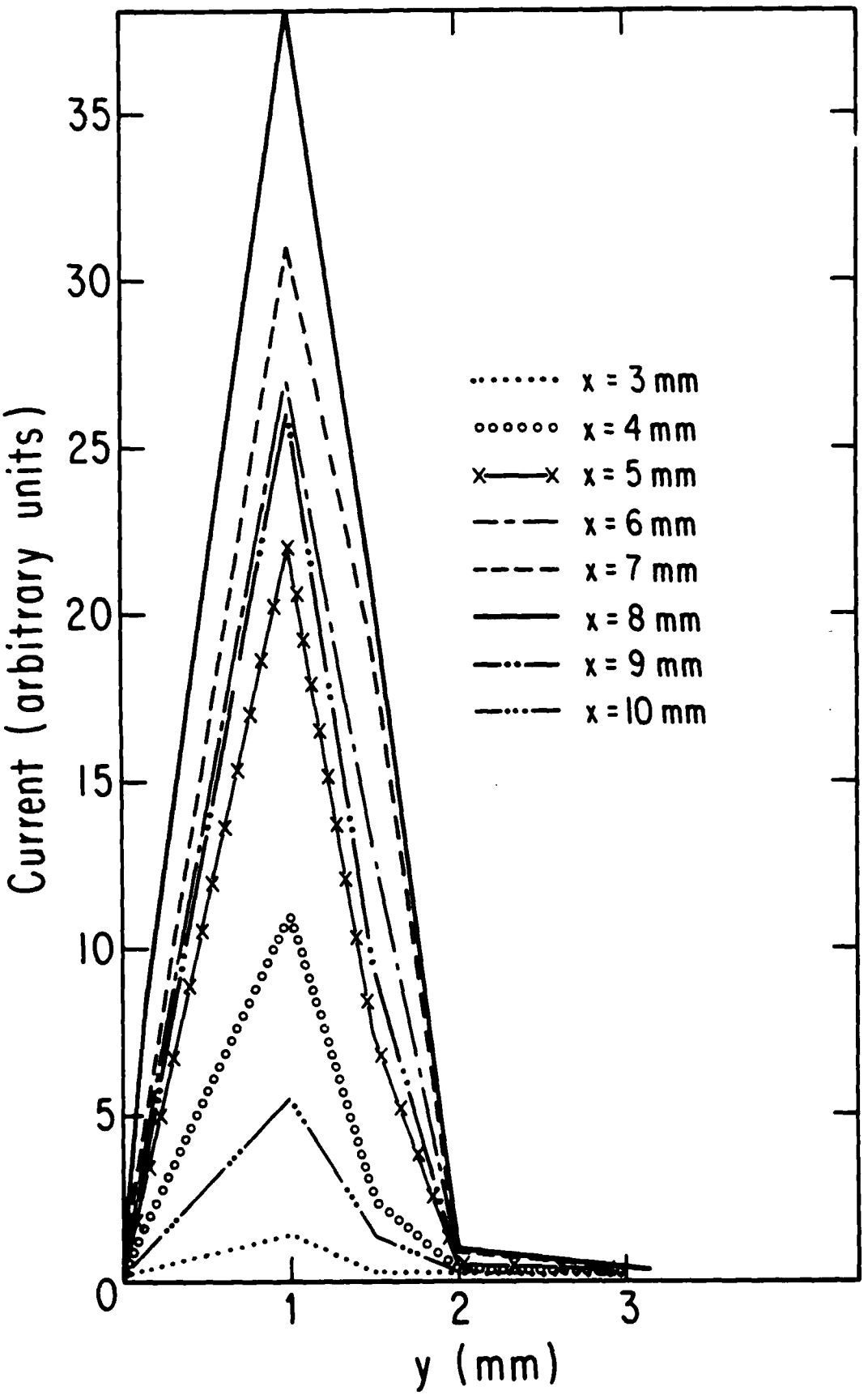
Current (arbitrary units)
35
30
25
20
15
10
5
0
1
2
3
y (mm)
x = 3 mm
x = 4 mm
x = 5 mm
x = 6 mm
x = 7 mm
x = 8 mm
x = 9 mm
x = 10 mm

Fig 7b

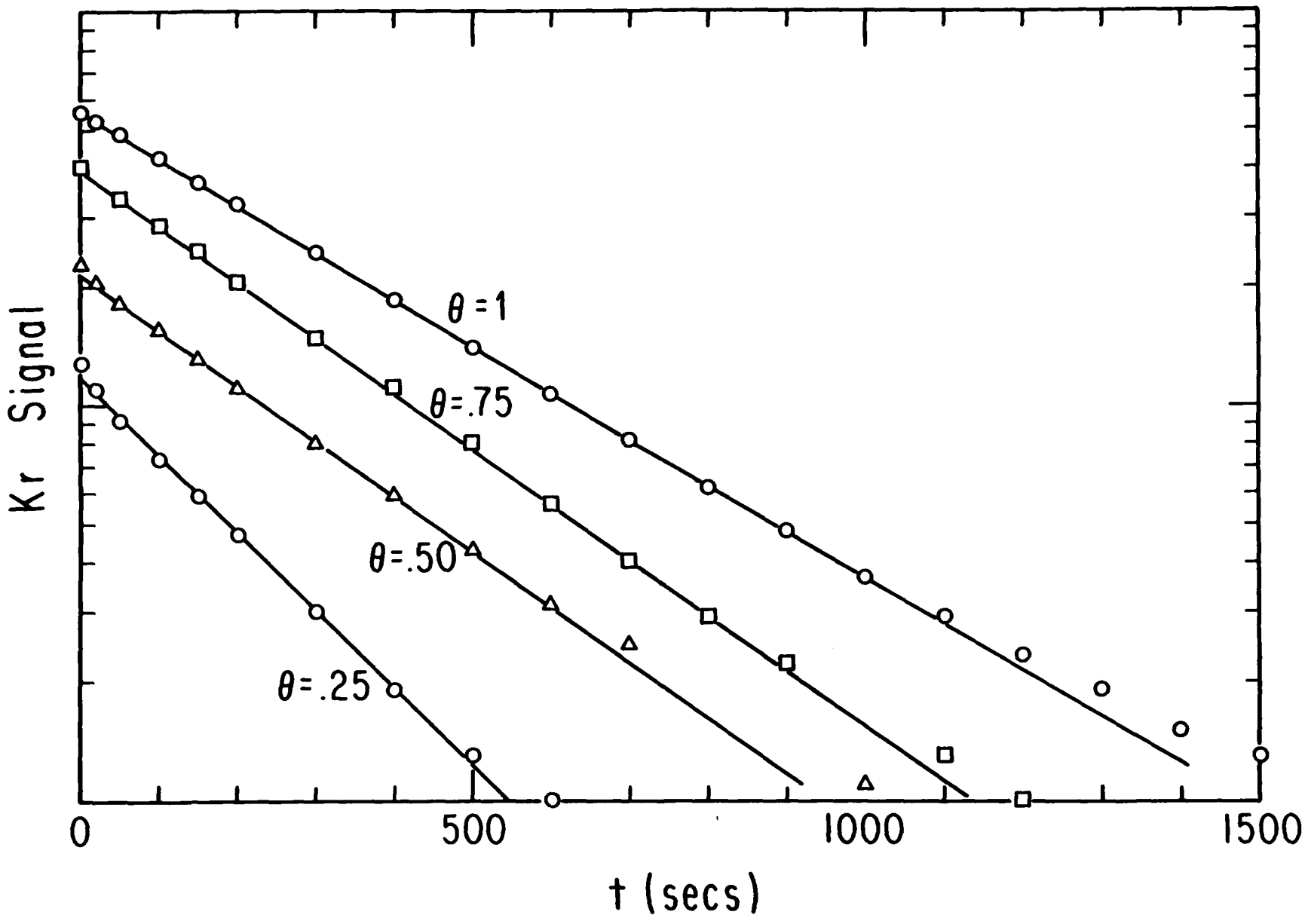

Fig 8.

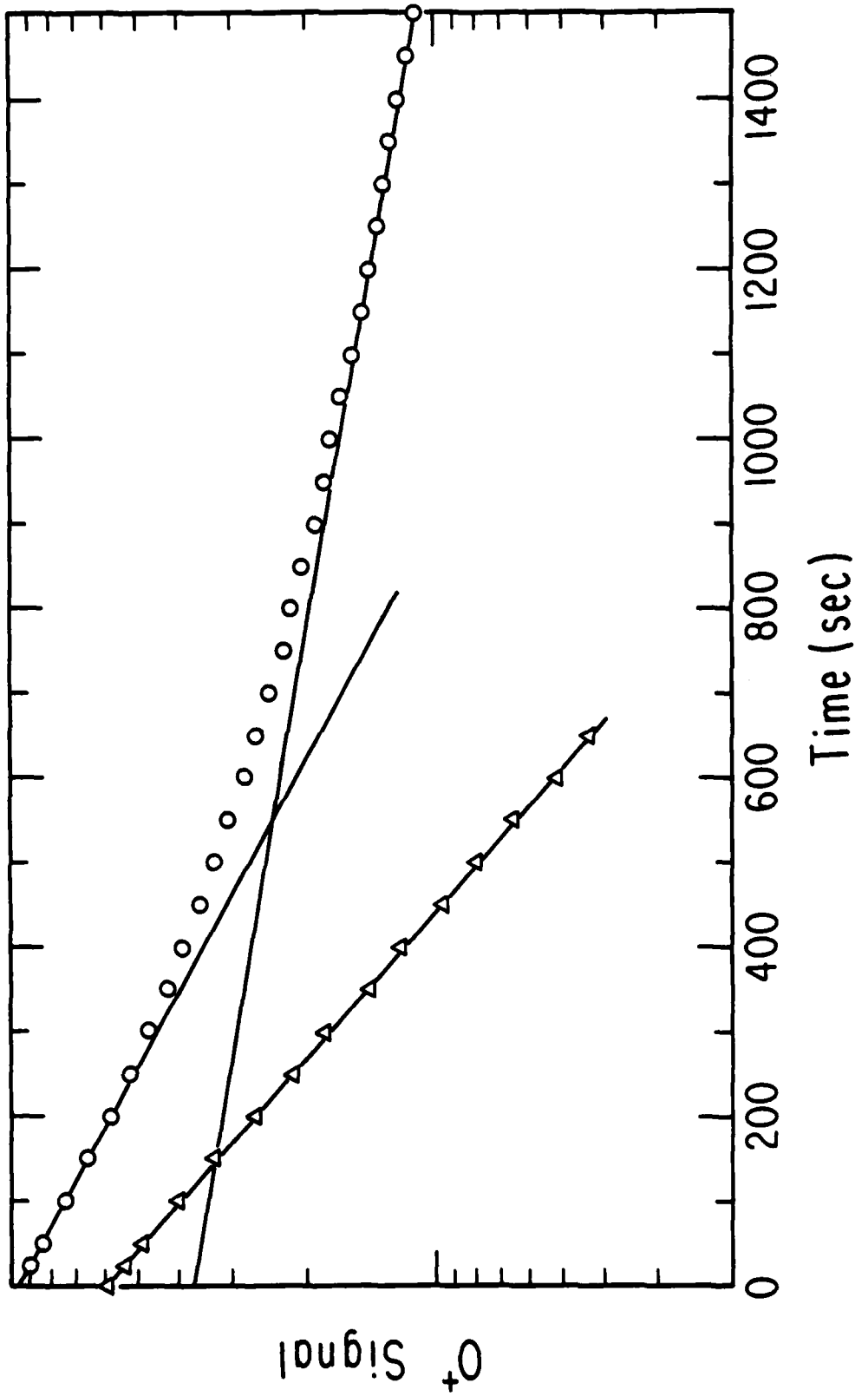

Fig 9

END

FILMED

3-86

DTIC